Twist localizes three-dimensional patterns

A. G. Rossberg*

Department of Physics, Kyoto University, 606-8502 Kyoto, Japan

A mechanism for the localization of spatially periodic, self-organized patterns in anisotropic media which requires systems extended in all three spatial dimensions is presented: When the anisotropy axis is twisted, the pattern becomes localized in planes parallel to the anisotropy axis. An analytical description of the effect is developed, and used to interpret recent experiments in the high-frequency regime of electroconvection by Bohatsch and Stannarius [Phys. Rev. E **60**, 5591 (1999)]. The localization width is found to be of the order of magnitude of the geometrical average of the pattern wavelength and the inverse twist.

PACS number(s): 45.70.Qj, 47.54.+r, 83.70.Jr, 44.27.+g

I. INTRODUCTION

Three-dimensional pattern formation in dissipative systems has been theoretically investigated to some extent for the case of the complex Ginzburg-Landau equation [1–6]—but there seems to be no experimental model for which the theory is quantitatively valid. Qualitatively, many results should also apply to a similar case, pattern formation in three-dimensional (3D) excitable media, for which controlled experimental realizations exist (see, e.g., Refs. [7–9]), although the containers are typically rather small. In both systems it seems reasonable to concentrate on the structure and dynamics of filaments formed by the cores of scroll waves, which largely control the dynamics in the remaining space. In a recent theoretical work, for example, the filament dynamics was investigated for an anisotropic excitable medium with a twisted anisotropy axis [10], a situation found in the human heart muscle. It was predicted that the filament typically drifts such as to align with the anisotropy axis.

Both the complex Ginzburg-Landau equation and excitable media exhibit traveling waves. For systems forming *stationarily bifurcating* spatially periodic structures, the dominance of the filaments formed by topological defects is not so strong, and different effects can be expected. A prototype for such a system might be the high-frequency regime of electroconvection (EC) in nematic liquid crystals. Convection patterns with a wavelength λ which is small compared to the spatial extensions of the sample are easily obtained, and sustained over long times by applying a sufficiently high ac voltage (with a modulation frequency higher than the ''cutoff frequency'' approximately equal to the inverse charge relaxation time) at plane, parallel (and transparent) electrodes enclosing the liquid crystal. However, there is still some discussion about whether the patterns are really three dimensional, i.e., arising from a bulk instability and forming a laminar structure, or rather parallel rolls located at the electrodes.

Closely related to this geometrical question is the question about the mechanism of convection. The most popular explanation, here called the standard model (SM), is by the dielectric regime of EC via the Carr-Helfrich mechanism (for de-

tails, see the references below), which is based on the Leslie-Ericksen formulation of nematodynamics. The SM predicts bulk convection. It has, on the linear level, been worked out by Dubois-Violette *et al.* [11]. Later it was modified for square-wave driving voltages [12], and to include flexoelectric effects [13–15] and the effects of finite cell thickness [16]. Recently it was extended to the nonlinear level [17]. But attempts to bring the predictions of the SM (threshold voltage and critical wave number) into quantitative agreement with experiments were only partly successful.

The main challenge to the SM is the ''isotropic'' mechanism for EC [18,19], for which the anisotropy of the nematic is only of secondary relevance. There, EC is driven by inverted charge gradients in thin Debye layers near the electrodes, which are not included in the SM. The isotropic mechanism naturally leads to boundary convection. Since several material parameters relevant to the isotropic mechanism are unknown, only semiquantitative predictions of the effect can be made.

In principle, both mechanisms are active, but it is reasonable to assume that one of them dominates. In a recent effort to settle the controversy on bulk vs boundary instability, Bohatsch and Stannarius [20] developed an experiment with a modified design, which was intended to map the structure across the cell onto the 2D shadowgraph image (or the diffraction pattern) of light passing through the cell.

The technique of Bohatsch and Stannarius was to use samples with a *twisted* geometry: just as in twisted nematic LCD displays, the anchoring of the nematic director $\hat{n}$ ($\hat{n}^2 = 1$) at the upper and lower electrodes (separation d) is such that $\hat{n}$ is parallel to the layer, but the alignment axis of the director at the upper boundary is perpendicular to that at the lower boundary. In the equilibrium configuration the director is planarly oriented, and interpolates between the boundaries with a uniform twist $\hat{n} \times \mathrm{rot}\, \hat{n}$. Configurations with positive or negative twists are thinkable. They are related to each other by a reflection. Without loss of generality, a negative twist ($-\pi/2d$) shall be assumed. Although inversion symmetry is broken in the twisted geometry, there is still the symmetry with respect to a 180° rotation of the cell around the axis of the director at midplane. The critical mode at the onset of EC, which breaks the approximate translation symmetry, can be symmetric with respect to this rotation (per-

haps followed by a translation by half a wavelength), leading to *normal rolls*, or also break this discrete symmetry, then leading to *oblique rolls*.

In experiments with untwisted cells, the rolls (or laminae) observed at the threshold of structure formation in the high-frequency regime are always normal.[1,2] Thus Bohatsch and Stannarius concluded by an intuitive argument, that, in twisted cells, the observation of normal rolls at threshold demonstrates a bulk instability, while the observation of oblique rolls is an indicator of a boundary instability, in particular when the rolls are approximately normal to the alignment of $\hat{n}$ at the boundaries. They observed a transition from normal to oblique rolls as the ac frequency increases.

Assuming that the SM is basically correct, Secs. II and III of this paper develop the linear theory for the convection pattern in twisted cells, predicting critical modes localized in planes far from or near to the electrodes, respectively, depending on the boundary conditions. Section IV sketches the nonlinear effects relevant at the threshold of convection, and Sec. V concludes with an interpretation of the experiments in light of the theory.

II. LOCALIZED BULK MODES IN THE STANDARD MODEL

Below, the linear theory of high-frequency EC in twisted cells is developed within the framework of the SM. The association of the obliqueness angle with the position of the convective mode turns out to be correct. But it is also found that the experimental results for twisted cells cannot be transferred to the untwisted cell, as suggested by Bohatsch and Stannarius, because the localization of the linear mode, near the boundaries or in the bulk, is enforced by the twist itself.

The calculations are based on the general weakly nonlinear theory [17] of dielectric EC in large containers, which has to take the interaction of the convection pattern with several homogeneous soft modes (hydrodynamic modes) explicitly into account. One of these modes is the director orientation. As follows from the general calculation, at lowest order, a twist does not excite the other soft modes of the liquid crystal, such as electric potentials or fluid motion, even when the electric ac voltage is applied. The direct influence of the twist on the convection pattern reduces to a purely geometric effect (no additional coupling constants not relevant for the untwisted cell are involved). The local amplitude and phase of the convection pattern is expressed by a complex field $A = A(x,y,z,t)$, such that the modulation of actual physical quantities u is given by $u(x,y,z,t) = u_0 A(x,y,z,t) \exp(iq_c x) + \text{c.c.} + (\text{higher order corrections})$, where q_c is the wave number of the convection pattern at threshold in the untwisted cell, and u_0 is a complex constant. The linear dynamics of A in the presence of a pure, not too strong twist of the nematic director is described [17] by

$$\tau \partial_t A = [\varepsilon + \xi_x^2 \partial_x^2 + \xi_y^2(\partial_y - iq_c\varphi)^2 + \xi_z^2 \partial_z^2]A. \quad (1)$$

---

[1] When chevron patterns are observed, one is not at the threshold of structure formation.

[2] In the low-frequency regime of EC they can be normal or oblique, however.

Here the z axis is perpendicular to the electrodes. To be specific, assume that $\hat{z}$ points ''up'' and $-\hat{z}$ points ''down.'' For now, the orientation of x and y axes relative to the director anchoring shall be left unspecified. This is possible because of the rotational symmetry underlying Eq. (1) [21]. The angle between $\hat{n}$ and the x-z plane is denoted by φ. The quantitative validity of Eq. (1) requires that φ be small, and that modulations of A and φ in space and time are slow. In particular Eq. (1) is never valid across the whole cell, since φ varies over an angle $O(1)$, a problem that will be discussed below. The (positive) coherence lengths ξ_x, ξ_y, and ξ_z are typically of the order $O(q_c^{-1})$, and τ is of the order of the charge relaxation time. The strength of the external stress is expressed by the reduced control parameter $\varepsilon := E^2/E_c^2 - 1$ in terms of the strength of the external electric ac field $E = V/d$ and the threshold field for electroconvection E_c for the thick ($d \to \infty$), *untwisted* cell. $|\varepsilon|$ is assumed to be small. (Observe that this definition of ε differs from the one used in Ref. [20], which is based on the threshold in the *twisted* cell with finite d, a quantity to be calculated below.) Analytic approximations for all quantities involved in description (1) can be found in Ref. [17].

The boundary condition corresponding to Eq. (1) is

$$A(x,y,z,y,t) = 0 \quad \text{at the horizontal boundaries.} \quad (2)$$

From the translation invariance in the x-y plane, it follows that the critical mode is of the form $A = a(z)\exp(iQx + iPy)$ with real Q and P, i.e., with a pattern wave vector $\vec{q} = (q_c + Q, P)$. We will *choose* the orientation of the x axis to be parallel to $\vec{q}$, in other words $P = 0$. It is easily seen by separation of variables that according to Eq. (1) the critical mode, i.e., the first mode to become unstable as ε increases, has $Q = 0$. It follows that the twist has no influence on the wavelength of the critical mode.

This result is in agreement with the measurements of Bohatsch and Stannarius for cells of intermediate thickness. But in their thinnest and thickest cells they found shorter wavelengths. While the deviation in the thin cell can be understood as a breakdown of the 3D amplitude formalism due to large spatial gradients of A and φ, the reason for the deviation in the thick cell is not clear. In agreement with theoretical expectations the wavelength decreases with increasing frequency. The observed deviation from the approximate $\lambda \sim \omega^{-1/2}$ law at the highest frequencies indicates that the wavelength has reached the Debye length and charge diffusion effects need to be taken into account in the theoretical description, an effect noticed already by Dubois-Violette *et al.* [11] (and typically to be expected at the $\sim 10^2$-fold cutoff frequency [17]).

Choose the origin of the z axis such that $\varphi = 0$ at $z = 0$. Denote by z_0 the distance of the lower boundary from $z = 0$ (i.e., the lower boundary is at $z = -z_0$). By the preceding construction, the amplitude of the critical mode is a function of z alone and satisfies

$$0 = [\varepsilon - \xi_y^2 q_c^2 \varphi^2 + \xi_z^2 \partial_z^2]A, \quad (3)$$

with $\varphi = \pi z/2d$. The equation has the form of the time-independent Schrödinger equation for the quantum harmonic oscillator.

Ignore, for a moment, the horizontal boundaries, and impose instead the boundary condition

$$A \quad \text{is bounded as} \quad |z| \to \infty. \tag{4}$$

Then the lowest eigenvalue of Eq. (3) is

$$\varepsilon = \varepsilon_c := \frac{\pi q_c \xi_y \xi_z}{2d}, \tag{5}$$

with a critical mode

$$A = \exp\left(-\frac{z^2}{2w^2}\right), \tag{6}$$

with a width

$$w = \left(\frac{2d\xi_z}{\pi q_c \xi_y}\right)^{1/2}. \tag{7}$$

Equations (5) and (6) correspond to the ground state of the harmonic oscillator.

Now assume $dq_c \gg 1$, which is required for the validity of Eq. (1). Then $\varepsilon_c = O(dq_c)^{-1} \ll 1$ and, within the range $|z| = O(w)$ covered by the critical mode, $\varphi = O(w/d) = O(dq_c)^{-1/2} \ll 1$. Thus, for $|z| = O(w)$, solutions (5) and (6) comprise a physically valid solution of Eq. (1). For $|z| \gg w$ the critical mode is to high accuracy zero, and thus a solution of the linear problem—also beyond the range of validity of Eq. (1). Of course any homogeneous boundary condition, in particular Eq. (2), is satisfied, provided the boundaries are sufficiently far away. Equations (5) and (6) therefore give a physically valid threshold and critical mode.

Next, consider the situation that one of two boundaries, e.g., the lower one, is near $z = 0$ [i.e., $z_0 = O(w)$], the other boundary far away. Then the lower boundary condition becomes

$$A = 0 \quad \text{at} \quad z = -z_0 \tag{8}$$

while the upper boundary condition effectively remains

$$A \quad \text{is bounded as} \quad z \to \infty. \tag{9}$$

This eigenvalue problem has to be solved numerically (after rescaling, it depends only on the parameters $\varepsilon/\varepsilon_c$ and z_0/w); here a shooting method is used. The lowest eigenvalue $\varepsilon(z_0)$ as a function of z_0 is shown in Fig. 2(b) (lower curve). As z_0 decreases to zero and the maximum of the critical mode approaches the boundary, the Gaussian shape of $A(z)$ is deformed, and the threshold $\varepsilon(z_0)$ increases monotonically. In particular, one finds $\varepsilon(0) = 3\varepsilon_c$, the eigenvalue of the first excitation and lowest antisymmetric mode of the "harmonic oscillator," with the corresponding eigenmode. Excitations near the boundaries have higher thresholds than in the bulk and are inhibited.

Thus the theory predicts that in thick enough cells the critical mode is localized within a horizontal layer which covers only a small fraction $O(w/d) = O(q_c d)^{-1/2}$ of the

cell. The orientation of the critical wave vector $\vec{q}$ and the position of the maximum of the critical mode within the sample are coupled, such that $\vec{q}$ is parallel to $\hat{n}$ at the maximum of $A(z)$. The orientation of the critical wave vector $\vec{q}$ lies between the two orientations of director anchoring at the boundaries. Small angles of order $O(w/d)$ between $\vec{q}$ and director anchoring are forbidden, but otherwise the orientation of $\vec{q}$ with respect to the symmetry axis, i.e., the obliqueness angle, is undetermined. One is thus dealing with a *highly degenerate problem* with critical wave vectors lying on a circular arc, similar to pattern formation in isotropic systems, where the critical wave vectors lie on a circle.

In thin cells, where $w/d, dq_c = O(1)$, the three-dimensional amplitude equation (1) is not an accurate description anymore. But when solved numerically with boundary condition (2) as a qualitative model, it predicts normal rolls in agreement with experiments.

The theoretical analysis for thick cells seems to correspond well with the observations of Bohatsch and Stannarius in the "broad" intermediate frequency range (within the high-frequency regime), where, near onset, the distribution of the wave-vector orientations is "broad, smeared out, and fluctuating" [20]. Unfortunately, no experimental raw data for this range have yet been published, which makes it hard to judge how well defined the maxima of these distributions are, which they *do* nevertheless find at small but finite obliqueness angles ($\approx 10°$), and which are difficult to understand from the theory presented here.

III. BOUNDARY MODES WITH MODIFIED BOUNDARY CONDITIONS

The experimental observation that, for frequencies above the intermediate "transition range," the distribution of the wave vectors near onset becomes narrower with maxima at obliqueness angles near $\pm 45°$, i.e., parallel to the surface anchoring, seems to be in contradiction with the theory based on the SM. A simple explanation for this, which should be examined experimentally before coming to a final conclusion, would be the combination of two effects. The first effect is that, at higher frequencies, where the pattern wavelengths are shorter and wave-optical effects have to be taken into account, the optical contrast of the shadowgraph method and the intensity of the reflexes in the optical far field become weaker. As a result, the apparent optical threshold of convection could lie slightly above the actual threshold. Wave-optical effects become important at a pattern wavelength λ of the order of magnitude of the geometrical average of the optical wavelength and the thickness of the convective layer $O(w) = O(\lambda d)^{1/2}$ [22], a condition satisfied in the present case. The second effect is that the value of the reduced control parameter corresponding to the onset of nontrivial, nonlinear behavior involving homogeneous soft modes scales like $(\lambda/d)^2$ or even $(\lambda/d)^4$ [17], and thus decreases with increasing frequency. In combination of these two trends, the observed large obliqueness angles near threshold in thick cells at high frequencies might, in fact, correspond to already fully developed nonlinear effects, such as the chevron pattern. In particular the obliqueness angles

above 45° (Ref. [20], Fig. 11, 3500 Hz) would then be easier to understand.

But one could also try to explain the observation of preferred obliqueness angles near $\pm 45°$ as a result of some mechanism of wave-vector selection that removes the degeneracy of the problem. Mostly linear selection mechanisms *via* perturbations from the boundaries shall be considered here. Nonlinear mechanisms will shortly be discussed in Sec. IV.

If there is a linear selection mechanism for large obliqueness angles at threshold, at least one of the three conditions (3), (8), and (9) must be invalid. The reason for this may be found in the truncation errors of the asymptotic expansion which leads to Eqs. (3), (8), and (9), the excluded effect of noise, or an insufficient description on the hydrodynamic level. All possible truncation errors become, in one way or another, large only for $z_0 = O(d)$. This will be demonstrated for one case below. If noise is the main cause for selecting z_0 (which is presumably the case at intermediate frequencies), it is reasonable to assume z_0 to be randomly distributed over $[0,d]$, leading again to $z_0 = O(d)$ on average. Thus it can be concluded that, in fact, the description on the hydrodynamic level, in particular near the boundaries, is insufficient.

For the eigenvalue problem considered above, boundary condition (8) turns out to be a somewhat singular case of the more general condition

$$A = \mu \partial_z A \quad \text{at} \quad z = -z_0, \tag{10}$$

with a real parameter μ. To discuss the implications of $\mu \neq 0$ as one possible truncation error or as a possible outcome of an extended hydrodynamic description, the eigenvalue problem (3) with boundary conditions (9) and (10) shall now be investigated. This will also yield an analytic argument, robust with respect to perturbations, that supports the numerical observation that for $\mu = 0$ the function $\varepsilon(z_0)$ is monotonously decaying with z_0.

Up to normalization, there is, for fixed ε, a single nontrivial solution $A(z) = f(\varepsilon, z)$ of Eq. (3) satisfying the upper boundary condition (9). The lower boundary condition (10) determines a discrete set of z_0 for given ε or, respectively, $\varepsilon = \varepsilon(z_0)$ is determined implicitly by the lower boundary condition as a multivalued function of z_0, i.e., by

$$f(\varepsilon(z_0), -z_0) = \mu f'(\varepsilon(z_0), -z_0), \tag{11}$$

where the prime on f denotes a differentiation with respect to the second argument.

At a local minimum of $\varepsilon(z_0)$ one has $\partial_{z_0}\varepsilon(z_0) = 0$, and differentiation of Eq. (11) with respect to z_0 yields

$$f'(\varepsilon(z_0), -z_0) = \mu f''(\varepsilon(z_0), -z_0). \tag{12}$$

By combining Eqs. (11) and (12) and the defining equation of f [Eq. (3)], one arrives at

$$\xi_z^2 f = \mu^2 \left[\frac{\pi^2 \xi_y^2 q_c^2 z_0^2}{4d^2} - \varepsilon \right] f. \tag{13}$$

For nonzero μ the common factor f can be canceled since $f \neq 0$ by Eq. (11). A simple algebraic relation between ε and z_0 (which determines the wave vector) for the critical mode is thus obtained.

As $\mu \to 0$, two cases can be distinguished. In the first case z_0 remains bounded. Then Eq. (13) reduces asymptotically to

$$\varepsilon \sim -\xi_z^2/\mu^2. \tag{14}$$

Corresponding solutions exist only for $\mu < 0$. They can be approximated by $f(\varepsilon, z) \approx \exp(z/\mu)$, and are strongly localized near the lower boundary. But due to the large values of $|\varepsilon|$ (as $\mu \to 0$), these solutions can not be expected to be always physically meaningful. In the second case z_0 increases over all bounds. Then small deviations from eigenvalue (5) and solution (6) are sufficient to satisfy the boundary conditions. Thus ε remains bounded, and Eq. (13) reduces asymptotically to

$$z_0 \sim \frac{2d\xi_z}{\pi q_c \xi_y |\mu|} = \frac{w^2}{|\mu|}. \tag{15}$$

In particular $z_0 \to \infty$ as $\mu \to 0$, supporting the numerical observation that $\varepsilon(z_0)$ is strictly monotonously decaying for $\mu = 0$.

It is easily verified that the analytic argument for $z_0 \to \infty$ as $\mu \to 0$ is, as far as physically interesting, robust against additions of higher order corrections of the form $g(\varphi^2)A$ to the right-hand side of Eq. (3) or the replacement of the term $\xi_z^2 \partial_z^2 A$ by some more precise form $h(\varphi^2)\partial_z^2 A$ [assuming that $h(\varphi^2)$ has no zeros for real φ, i.e., the partial differential equation is nonsingular]. All other higher order corrections to Eq. (3) involve higher order derivatives (and additional boundary conditions). If these corrections are small they are, in a first approximation, active only in a thin boundary layer and lead, effectively, to modified boundary conditions of the form of Eq. (10). Thus, taking the validity of the upper boundary condition (9) for granted, a modified lower boundary condition is always involved in a localization near the lower boundary.

To better understand the situation for $\mu \neq 0$, a numerical solution of the problem is required. Figure 1 shows numerical results for the values of ε and z_0 at threshold [i.e., the minimum of $\varepsilon(z_0)$] for finite μ. Although in the limit $\mu \to 0$ numerics break down, the asymptomatic results are reproduced for small μ. The calculations also show that for $\mu > 0$ the minima of $\varepsilon(z_0)$ lie below the bulk ($z_0 \to \infty$) value ε_c as expected, but for $\mu < 0$ are, on the starred branch (see Fig. 1), above ε_c. A look at the function $\varepsilon(z_0)$ (Fig. 2) shows that for negative μ the minima on the starred branch belong to the branch of $\varepsilon(z_0)$ which approaches $3\varepsilon_c$ as $z_0 \to \infty$. It also becomes clear that the existence of the minima of $\varepsilon(z_0)$ for $\mu < 0$ is closely related to the existence of the thin boundary mode corresponding to eigenvalue (14): The minima result from the avoided crossings of the spectrum of the modes localized near $z = 0$, which have decreasing eigenvalues for increasing z_0, and the eigenvalue of the thin boundary mode, which increases with z_0. If the thin boundary mode is an unphysical artifact of the boundary conditions, the minima in the function $\varepsilon(z_0)$ are also unphysical. This point can be demonstrated by using the original bound-
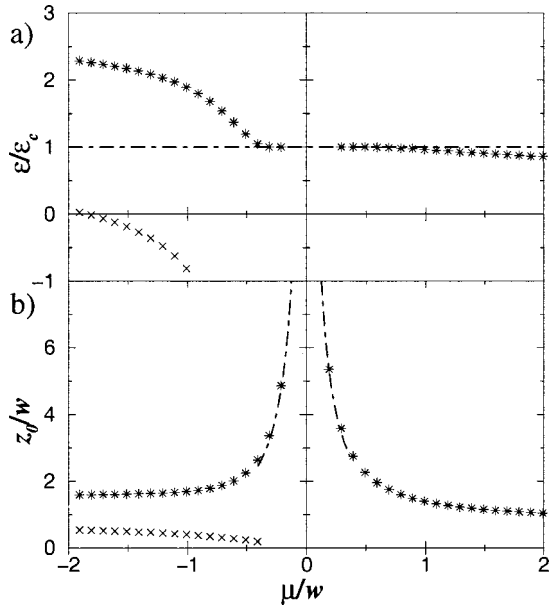
FIG. 1. (a) The threshold value of dielectric electroconvection (relative to the bulk threshold in an untwisted nematic) in units of ε_c [Eq. (5)] and (b) z_0 (approximately equal to the distance of the maximum of the critical mode from the boundary) in units of the width w of the critical mode [Eq. (7)], both as functions of the parameter μ in boundary condition (10). Stars and crosses are numerical solutions. The crosses correspond to a thin boundary mode. The dashed lines are the analytical approximations for small $|\mu|$, Eq. (15) for (b).

ary condition [Eq. (8)] as the lower boundary condition and adding, to model the mixed boundary condition (10), a term $b(z+z_0)\partial_z A$ to the l.h.s. of Eq. (3), where $b(z)$ is, e.g., given by

$$b(z) = \begin{cases} 13.2\varepsilon_c w \mu & \text{if } z < 2.83w \\ 0 & \text{otherwise.} \end{cases} \quad (16)$$

With these modifications the thin boundary mode—and therefore the avoided crossings and the minima of $\varepsilon(z_0)$—are suppressed for $\mu < 0$, but otherwise the spectra change only little (see Fig. 2).

Can higher order corrections to the boundary conditions that arise from the asymptotic expansion *in the framework of the SM* explain the preference of large obliqueness angles? From the figure in Ref. [17] displaying the hydrodynamic boundary layer of dielectric electroconvection, a value $\mu \approx -0.4 q_c^{-1}$ can be obtained. The sign follows directly from the fact that convection is suppressed by the no-slip boundary conditions for the hydrodynamic velocity field, the order of magnitude follows from the geometry of the flow. By the sign of μ a preference of large obliqueness angles (boundary instability) is excluded. Even if the sign would change but the magnitude remain the same, Eq. (15) would give an unphysical value $z_0 > d$.

IV. NONLINEAR SELECTION

In principle a nonlinear selection of large obliqueness angles is also conceivable. At threshold, two kinds of nonlinear mechanisms are active [17]. The first is the direct,
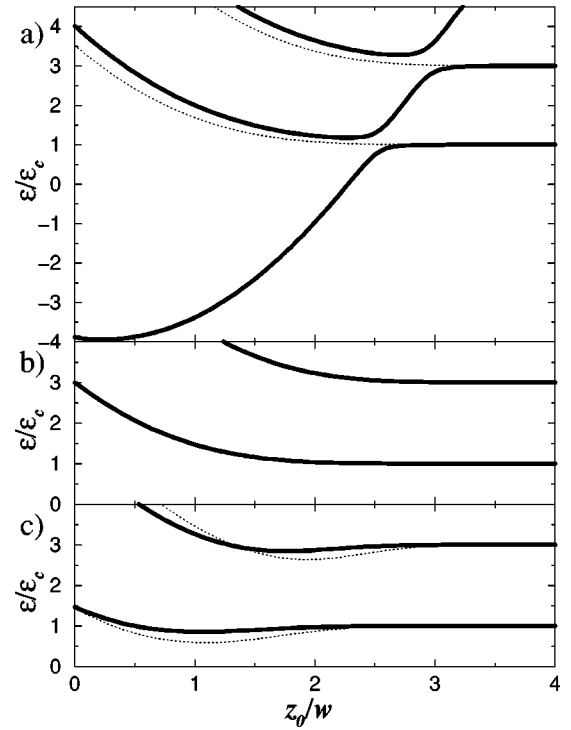

FIG. 2. The lowest eigenvalues $\varepsilon(z_0)$ for (a) $\mu = -0.5w$, (b) $\mu = 0$, and (c) $\mu = 2.0w$. The solid lines correspond to the eigenvalue problem [Eqs. (3), (8), and (9)], and the dotted lines to a modified model that does not contain the boundary mode leading to the large negative eigenvalues $\varepsilon(z_0)$ for negative μ. For $\mu = 0$, solid and dotted lines are identical.

local, nonlinear saturation of the pattern amplitude, the strength of which is measured by the coefficient g in Ref. [17]. This mechanism inhibits the coexistence of linear modes of the form of Eq. (6) if the overlap of the two modes along z is too large. Correspondingly, the wave vectors of coexisting linear modes can be expected to enclose some finite minimum angle. This could, for not too small a value of w/d, lead to the preference of certain wave-vector combinations which fill the allowed range of $\approx \pm 45°$ particularly well, but it does not imply that large obliqueness angles are generally preferred.

The second nonlinear mechanism acts indirectly *via* the electric potential. At positions in the sample where $|A|^2$ is large, additional charge transport processes are active, which effectively increase (S_E in Ref. [17] is positive) the electrical conductivity. Consequently, the strength of the electric driving field is reduced where $|A|^2$ is large and increased where $|A|^2$ is small, under the constraint that the total voltage drop is constant. But this effect is typically weak compared to direct nonlinear suppression, and presumably does not change the qualitative properties of the planform selection problem.

V. CONCLUSION

It was shown that a twist of the nematic director—or another anisotropy axis in a different system—leads to a localization of the pattern in planes parallel to the director. When the twist is not too strong, the localized linear modes can be calculated in the framework of the amplitude formalism. In

electroconvection, apart from being the twist axis, the z axis in Eq. (1) plays another special role—the external electric field is parallel to $\hat{z}$. But little would change if this additional anisotropy was missing (e.g., for reaction-diffusion patterns in uniaxially anisotropic media). Only ξ_y and ξ_z would then be equal by symmetry.

For dielectric EC in twisted nematic cells the localization width $w = O(d/q_c)^{1/2}$ is given by Eq. (7). When the material parameters of the liquid crystal are known, w can be calculated using the analytic approximations for the coherence lengths and the wave number from Ref. [17]. As a result of the localization, the critical wave vector is degenerate on a circular arc. The angle enclosed by the arc might be increased beyond 90° by using supertwist nematic cells. One then obtains a pattern-forming system with a geometry very similar to a two-dimensional isotropic system, but with a different topology (no invariance of the pattern under 180° rotation) and very particular nonlinear interactions.

The observation of normal rolls in thin cells and at low frequencies (large wavelength) by Bohatsch and Stannarius [20] is compatible with—and presumably predictable from— the standard model. The transition to a state with a ''broad, smeared out, and fluctuating'' distribution of wave-vector orientations at higher frequencies can be understood from the wave-vector degeneracy. The theory also reproduces their observation that the transition takes place at some more or less fixed ratio λ/d. This corresponds to some fixed ratio w/d at which boundary condition (4) becomes appropriate and degeneracy sets in. Assuming that the observations at yet higher frequencies, where the wave vectors were better defined and aligned with the director anchoring, did not suffer from the technical difficulties described in the beginning of Sec. III, they seem to exhibit effects not described by the standard model. These effects seem to lead effectively to modified boundary conditions of the form of Eq. (10), with $\mu > 0$. Nevertheless this does not imply that, just as in the twisted cell, there are boundary modes also in the untwisted cell. Solution of the linear problem for the untwisted cell with boundary condition (10), $\mu > 0$, and a corresponding upper boundary condition yields a critical mode covering the whole cell. Since the theory can explain the transition at the lower end of the intermediate-frequency range with fluctuating wave vector but does not imply that there is another transition at an upper bound, it may also be useful to investigate the two transitions independently in experiments. The intermediate-frequency range is probably an independent regime, and not just as the crossover between the low-frequency and the high-frequency range.

Conclusive information on the 3D structure of the high-frequency mode in untwisted cells might be obtained by investigating spectrally resolved shadow graphs or light scattering.

[1] J. P. Keener, Physica D **31**, 269 (1988).

[2] T. Frisch and S. Rica, Physica D **61**, 155 (1992).

[3] M. Gabbay, E. Ott, and P. N. Guzdar, Phys. Rev. Lett. **78**, 2012 (1997).

[4] O. Törnkvist and E. Schröder, Phys. Rev. Lett. **78**, 1908 (1997).

[5] I. S. Aranson, A. R. Bishop, and L. Kramer, Phys. Rev. E **57**, 5276 (1998).

[6] G. Rousseau, H. Chate, and R. Kapral, Phys. Rev. Lett. **80**, 5671 (1998).

[7] B. Welsh, S. Gomatam, and A. Burgess, Nature (London) **304**, 611 (1983).

[8] W. Jahnke, C. Henze, and A. Winfree, Nature (London) **336**, 662 (1988).

[9] M. Vinson, S. Mironov, S. Mulvey, and A. Pertsov, Nature (London) **386**, 447 (1997).

[10] M. Wellner, O. Berenfeld, and A. M. Pertsov, Phys. Rev. E **61**, 1845 (2000).

[11] E. Dubois-Violette, P. D. Gennes, and O. Parodi, J. Phys. (Paris) **32**, 305 (1971).

[12] I. W. Smith *et al.*, J. Phys. (Paris), Colloq. **36**, C-237 (1975).

[13] N. V. Madhusudana and V. A. Raghunathan, Liq. Cryst. **5**, 1789 (1989).

[14] W. Thom, W. Zimmermann, and L. Kramer, Liq. Cryst. **4**, 309 (1989).

[15] L. Kramer *et al.*, Liq. Cryst. **5**, 699 (1989).

[16] L. Kramer and W. Pesch, in *Pattern Formation in Liquid Crystals*, edited by A. Buka and L. Kramer (Springer, New York, 1995).

[17] A. G. Rossberg, e-print nlin/0001065.

[18] M. I. Barnik, L. M. Blinov, S. A. Pikin, and A. N. Trufanov, Zh. Éksp. Teor. Fiz. **72**, 756 (1977) [Sov. Phys. JETP **45**, 396 (1977)].

[19] V. G. Chigrinov and S. A. Pikin, Kristallografiya **23**, 333 (1978); [Sov. Phys. Crystallogr. **23**, 184 (1978)].

[20] H. Bohatsch and R. Stannarius, Phys. Rev. E **60**, 5591 (1999).

[21] A. G. Rossberg, A. Hertrich, L. Kramer, and W. Pesch, Phys. Rev. Lett. **76**, 4729 (1996).

[22] A. G. Rossberg, 1998 (unpublished).